JARO 01: 283–291 (2000)
DOI: 10.1007/s101620010048

JARO
Journal of the Association for Research in Otolaryngology

Two Models of Outer Hair Cell Stiffness and Motility

PETER DALLOS AND DAVID Z.Z. HE

Auditory Physiology Laboratory (The Hugh Knowles Center), Departments of Neurobiology and Physiology and Communication Sciences and Disorders, Northwestern University, Evanston, IL 60208, USA

Received: 12 May 2000; Accepted: 14 September 2000; Online publication: 31 January 2001

ABSTRACT

Cochlear outer hair cells change their axial dimension and theiraxial stiffness when their membrane potential is altered. These changes appear to be highly correlated. Because of this, we endeavored to produce models that would yield both phenomena via a single mechanism. Two models are proposed. In one, it is assumed that elementary motor molecules can be in either of two conformational states, these having different physical lengths and stiffnesses. The state of the molecule is taken to be a stochastic function of membrane potential and is expressed by a Boltzmann relationship. In the other model, a similar dependence is assumed to occur between membrane potential and stiffness, but no dimensional change isassigned to the molecule. Length changes can be had by preloading the cell. We show that either general model can produce realistic length and stiffness changes with an appropriate selection of parameters. One particular realization of the first model is proposed as an example. In this—the boomerang model—the molecule is assumed to be ℒ-shaped, with two different angles between the two legs representing the conformational states. Finally, the behavior of the model is compared with available data when the voltage stimulus comprises a brief sinusoid upon a DC pedestal.

INTRODUCTION

Cochlear outer hair cells are epithelial cells with a cylindrical shape. Upon change of their membrane potential, they undergo a change of axial length (electromotility; Brownell et al. 1985; Kachar et al. 1986; Ashmore 1987). We have recently discovered that the axial stiffness of isolated mammalian outer hair cells (OHC) is also voltage dependent. Using both microchamber (Evans et al. 1989) and whole-cell voltage-clamp (Hamill et al. 1981; Ashmore and Meech 1986) techniques, it was demonstrated that cell stiffness increases upon hyperpolarization and decreases when the cell is depolarized (He and Dallos 1999, 2000). The stiffness change can be quite large—of the order of 100%. One interesting finding is that stiffness change and electromotility appear to covary if manipulated. For example, the frequency dependence of both processes follows similar patterns (Dallos and Evans 1995). Also, when motility is reduced by the use of gadolinium (Santos–Sacchi 1991), stiffness change is also reduced. We also previously reported that the modulatory effect of acetylcholine upon electromotility can be explained by a reduction of the cell's internal stiffness upon application of the neurotransmitter (Dallos et al. 1997). The question naturally arises whether it is possible to explain the voltage-dependent stiffness and motility by a single mechanism. We develop two generic models here. In the first, it is assumed that molecular motors change both their axial dimension and stiffness upon a voltage-dependent conformational shift. In the second model, only a stiffness change is associated with elementary motors. Corresponding cell-length change is obtained if the quiescent cell is preloaded so that in its resting state it is shorter than its natural length. One particular realization of the first model is also proposed. The simple models developed here seem capable of producing realistic stiffness and motility patterns. They also naturally provide for covariance of axial cell stiffness and cell length. A preliminary account has already been published (Dallos and He 2000).

Correspondence to: Dr. Peter Dallos • Northwestern University • 2299 North Campus Drive • Evanston, IL 60208. Telephone: (847) 491-3175; fax: (847) 467-4327; email: p-dallos@northwestern.edu

RESULTS

Stiffness/length-change model

We first consider the relationship between molecular state and driving voltage and then compute the whole cell's stiffness and length as a function of this voltage. Assume that elementary motors are allosteric proteins that have two states designated **S** and **L**. Corresponding to the two states, the molecule presents two axial stiffnesses K_S and K_L. Also corresponding to the two states, the molecule has axial dimensions of X_S and X_L. In other words, the elementary motor changes both its linear axial dimension and its axial stiffness as it undergoes conformational changes. The probability of an elementary motor being in its **S** state (p_S) depends on the change in cell-membrane potential via the following Boltzmann function:

$$p_S = \frac{1}{1 + e^{(-aV+b)}} \tag{1}$$

where V is the deviation from the resting membrane potential (i.e., the command voltage) and a and b are constants. Assume that the cell's radius is r, its resting (zero command voltage) length is L, the resting linear packing density of motor molecules is Q (in both axial and circumferential dimensions), and that the cell is a simple cylinder. The total number of motors in a given axial dimension is $N_L = LQ$. These elements are in series; consequently, it is the reciprocal of their stiffnesses that sum to yield the reciprocal of the total stiffness of such a line of elements. Along the cell's circumference, there are $N_r = 2\pi rQ$ such axial lines of motors, and the stiffnesses of these sum to yield the total axial stiffness of the cell. Using these relationships, the following equations represent the global axial stiffness and length of the cell:

$$K_{\text{cell}} = \frac{N_r}{N_L}\left[K_S\, p_S + K_L(1 - p_S)\right] \tag{2a}$$

$$L_{\text{cell}} = N_L\left[X_S\, p_S + X_L(1 - p_S)\right] + L_0 \tag{2b}$$

The above model represents the simplest possible configuration. It consists of stacked-up motor proteins, without additional elastic elements connecting them, as envisioned before (Dallos et al. 1992, 1993, 1997). Thus, the total stiffness is made up of the summed motor stiffnesses, and the total length is the sum of the controllable motor lengths plus some constant length L_0. At $V = 0$, $L_{\text{cell}} = L$. The orientation of all motors is assumed to be identical *vis-à-vis* the long axis of the cell. It is a relatively simple matter to incorporate additional elementary "springs" connecting the motors and also other global elastic elements. We now proceed to include additional elements in the model. Figure 1 shows the equivalent mechanical circuit used in these computations. The apparent axial stiffness of the motor molecule is K; of course, K has two possible values, K_S and K_L, depending on its state, **S** or **L**. Adjacent elementary motors are axially connected by springs of stiffness κ, and the parallel global stiffness (not related to the elementary motors) is λ. No restraint is assumed between adjacent motors along the circumferential dimension. The cell's total axial stiffness is K_{cell}:

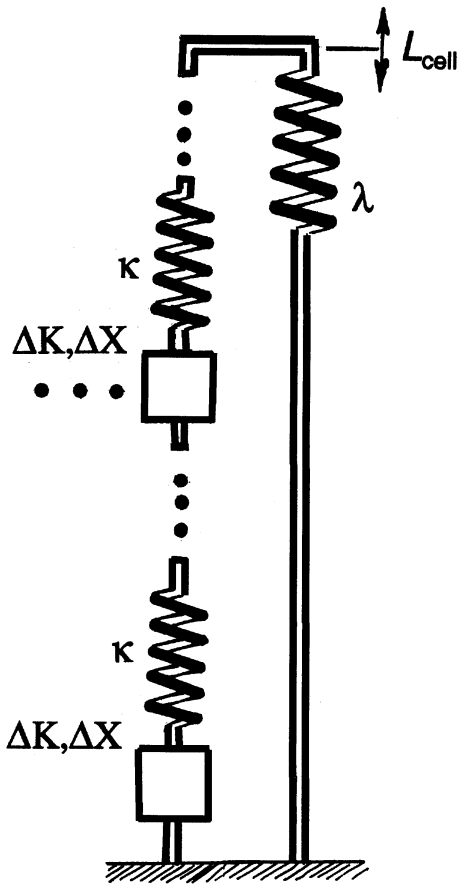

FIG. 1. Depiction of the whole cell's mechanical circuit. This consists of a stack of QL components, each connected by elementary springs κ and parallel to a global spring λ. The boxed components, symbolized as (ΔK, ΔX), represent the molecular motors that change their length and stiffness. At any given axial location, there are $2\pi rQ$ (ΔK, ΔX) and κ units along the cell's circumference. At any given circumferential location, there are LQ such units along the length of the cell.

$$K_{\text{cell}} = \lambda + \frac{N_r}{N_L}\left[\frac{\kappa K_S}{\kappa + K_S}\, p_S + \frac{\kappa K_L}{\kappa + K_L}\,(1 - p_S)\right] \tag{3}$$

The total axial stiffness is a stochastic function of membrane potential via eq. (1). We now compute the total

cell length with the aid of eq. (2) in Dallos et al. (1997) and eq. (2b) above:

$$L_{\text{cell}} = L_0 + N_r N_L \kappa \left[\frac{K_S p_S X_S}{N_r \kappa K_S + N_L \lambda(\kappa + K_S)} + \frac{K_L (1 - p_S) X_L}{N_r \kappa K_L + N_L \lambda(\kappa + K_L)} \right] \quad (4)$$

The two terms in brackets in eq. (4) correspond to the summed lengths of the motors, weighted by the associated stiffnesses in their **S** and **L** states. This is the controllable length, while L_0 is the axial dimension extraneous to the mobile portion of the motors.

Let us take some judiciously chosen parameter values, partially based on our experimental results (He and Dallos 2000), and compute the resulting dependence of stiffness and length upon command voltage. While the parameter choices below appear arbitrary, we show below that when a specific model is introduced to embody the present version of the model, the numbers prove to be both reasonable and self-consistent. We take the representative values of $K_{\text{cell}} = 7$ mN m^{-1} at $p_S = 0$ and $K_{\text{cell}} = 0.7$ mN m^{-1} at $p_S = 1$, and a consistent set of numbers: $\kappa = 70$ mN m^{-1}, $K_L = 15$ and $K_S = 0.2$ mN m^{-1}. The packing density of the molecules is taken as $Q = 80$ μm^{-1}, hence $N_r = 2512$ and $N_L = 4800$ for a 60-μm-long, 10-μm-diameter cell. A value for the global cell stiffness λ is taken as one-tenth of the cell's resting stiffness, or 0.6 mN/m. We further assume that $X_L = 1$ and $X_S = 0.65$ nm, with an excursion ("throw") of the elementary motor ($X_L - X_S$) of 0.35 nm. The parameters a and b in the Boltzmann function are taken as 0.075 mV^{-1} and 1.5 in order to yield a functional shape that resembles the experimental data (Dallos et al. 1993). These parameters yield $p_S = 0.18$ at $V = 0$.

In the resting state, i.e., at $V = 0$, the uncontrolled length (L_0) is chosen as 56.3 μm to yield $L_{\text{cell}} = L = 60$ μm at $V = 0$ [from eq. (4)]. Total stiffness and total cell length as functions of the command voltage are depicted in Figure 2A, B. Note that the resting global stiffness is ~6 mN/m, which is similar to the average value that we find experimentally. Over the command-voltage swing represented on the abscissa, the cell stiffness changes between approximately 7 and 0.8 mN m^{-1}. Over the same range of potential swing, the cell length varies between approximately 61 and 57 μm. To better appreciate these relative ranges of change, we plot them as percentages in Figure 2C. It is apparent that while length changes only a small relative amount (~6%; this is, of course, due to the small fraction of controlled vs. constant axial cell dimensions), stiffness changes exceed 100%. Both of these values are in line with experimental observations (He and Dallos 1999, 2000).

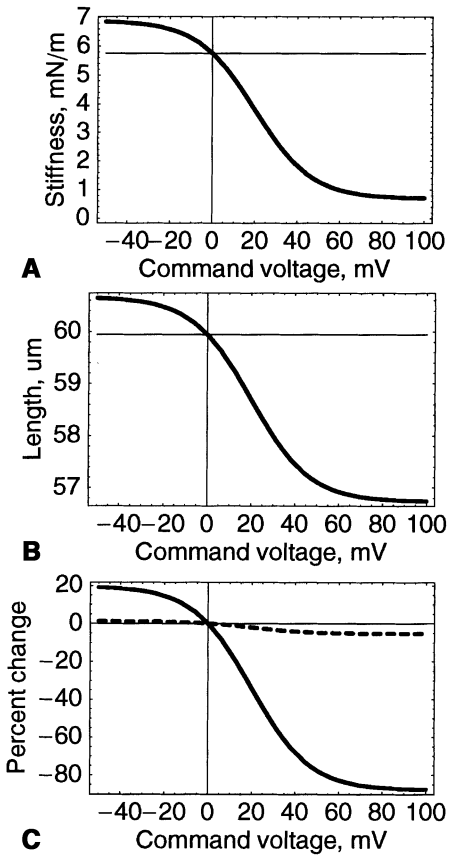

FIG. 2. **A** Absolute cell stiffness as a function of membrane-potential change around the cell's resting potential. Computation is based on eqs. (1), (3), and (4). The parameters used to obtain these curves are stated in the text. **B**. Absolute length, computed as above. **C**. Same as above, except that changes from resting values (stiffness and length) are expressed as percentages. Solid line = stiffness, dotted line = length.

The prestressed spring model

We emphasize that the above model is not the only possible means of achieving joint length and stiffness change with a single mechanism. An attractive alternative is based on the assumption that the motor molecule does not undergo any direct length change. Instead, the **S** state is again associated with an elementary stiffness K_S, whereas the **L** state produces K_L. Then eq. (3) can still describe the cell's axial stiffness. Motility can be produced if the cell is preloaded, either internally or externally. It is emphasized that this variant of the model assumes no conformational length change of the motor molecule or a driven change of the cell's surface area. The motor simply functions as a variable (two-state) elementary stiffness unit. Thus, stiffness change is the primary variable, while motility ensues as a byproduct of stiffness, change.

Assuming that a displacement source (x_0) of internal stiffness ρ compresses the cell, the length change can be expressed as follows:

$$\Delta X_{\text{cell}} = x_0 \frac{\rho}{\rho + K_{\text{cell}}(0)} \left[\frac{K_{\text{cell}}(0)}{K_{\text{cell}}(V)} - 1 \right] \quad (5a)$$

where $K_{\text{cell}}(V)$ is the cell's stiffness at command voltage V and $K_{\text{cell}}(0)$ is its stiffness in the quiescent state (at $V = 0$). Clearly, as K_{cell} is modulated [eq. (3)], so is the cell length. If for simplicity we assume an ideal displacement source (i.e., $\rho \to \infty$), the equation is simplified:

$$\Delta X_{\text{cell}} = x_0 \left[\frac{K_{\text{cell}}(0)}{K_{\text{cell}}(V)} - 1 \right] \quad (5b)$$

An extremely modest preload (x_0) of approximately 0.6 μm is sufficient to yield realistic length changes (~0.4 μm maximum extension and ~4.4 μm maximum contraction) if stiffness varies as in Figure 2A. Thus, if the stiffness of the elementary motor changes between the two states, just as in the model considered previously, $K_S = 0.2$ mN m^{-1} and $K_L = 15$ mN m^{-1}, a modest preload will yield appropriate length changes. In order to obtain the proper sign for dimensional changes, the cell needs to be compressed in the quiescent state. Then, depolarization causes a decrease in stiffness and shortening, while hyperpolarization increases cell stiffness and this, in turn, produces lengthening.

The boomerang model

As an example, we now develop a specific embodiment of the model discussed in the "Stiffness/length-change model" subsection above, in a form where the elementary motor produces both stiffness and length changes. In earlier work (Dallos et al. 1992, 1993), we made use of the concept of motility being driven by the stochastic behavior of a large number of elementary "motor molecules." It was assumed that individual motors are allosteric membrane-spanning proteins that have two stable states, short or small (**S**) and long or large (**L**); hence, the nomenclature adopted here. The probability of being in a given state was determined by Boltzmann statistics, with membrane potential as the controlling variable. Several cartoons were provided to suggest conceivable shapes for the motor in its two states. Analogous with the all-*trans* to 11-*cis* transformation of the chromophore retinal, one suggested a boomerang-shaped configuration with a variable angle between the two arms. Our present modeling effort begins with such a shape change.

Figure 3 shows the proposed configuration of the motor molecule. The angle between the two arms is α in the **L** state and β in the **S** state. Thus, $\Phi = \alpha - \beta$, the conformational angle change that corresponds to transformations between the **L** and **S** states. Change from **L** to **S** state and back is again assumed to be a

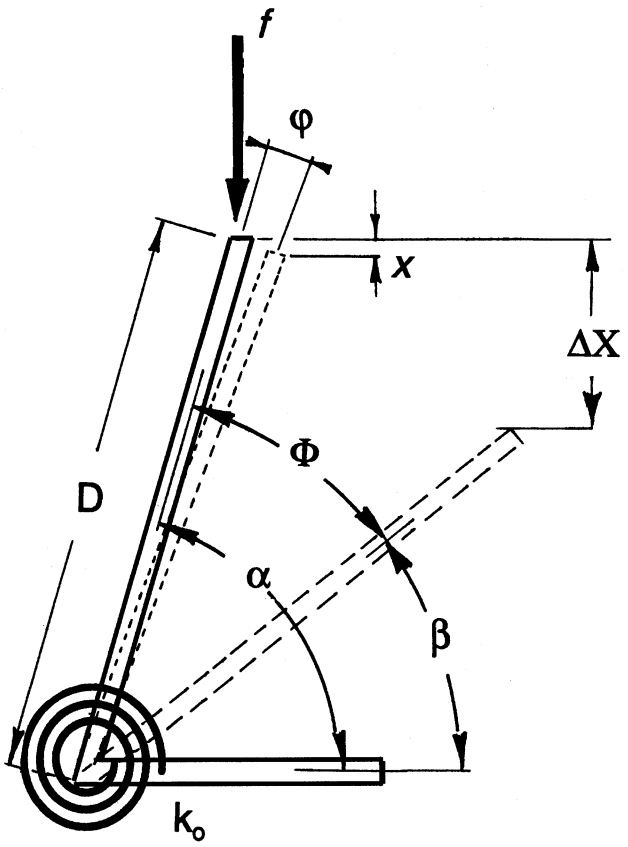

FIG. 3. Boomerang model of the molecular motor. In one of its states (**L**), the molecule is shown with solid contours, whereas in its other state (**S**), it is shown with dashed lines. The resting angle between the arms of the molecule is α, whereas that in the active state is β. Thus, the conformational angle change is $\alpha - \beta = \Phi$. The two arms are connected with a rotational elasticity k_0. If an external force f acts on the movable arm along the main axis of the cell, it will rotate the arm through a small angle ϕ. This will produce a dimensional change X of the molecule along the cell's main axis. The apparent stiffness change of the molecule is then f/x. A conformational shift of the molecule produces axial length change ΔX and a corresponding stiffness change ΔK. It is assumed that all molecules line up along the surface of the cell oriented so that the force f is axial.

stochastic function of voltage [eq. (1)]. The two arms are connected with a "coil spring" whose rotational stiffness is k_0. It is assumed that because of external force, limited rotation of the arm is permitted around either state, but that angular rotations equivalent to those occurring during a conformational change event cannot be imposed by an extrinsic force. This constraint is made because experimental evidence indicates (He and Dallos 2000) that the cell's axial stiffness is essentially linear with externally imposed length change. If in the **L** state a force f, perpendicular to the lower arm, is applied to the tip of the upper arm of length D, then the arm will rotate through an angle φ. A torque [$T = Df\cos(\alpha - \varphi)$] is exerted upon the spring.One can express the angle φ as $\varphi = T/k_0$. From the vantage point of the applied force, the *apparent*

stiffness is $K = f/x$, where x is the small vertical displacement of the tip of the upper arm: $x = D\,[\sin\alpha - \sin(\alpha - \varphi)]$. The stiffness K can now be expressed in terms of the angles α and φ:

$$K = \frac{\varphi \mathbf{k}_0}{D^2 \cos(\alpha - \varphi)[\sin\alpha - \sin(\alpha - \varphi)]} \qquad (6)$$

Recall that the assumption is that only small rotations resulting from external force are permitted. Consequently, in the limit, based on $\varphi \to 0$, one obtains for the apparent stiffness in the **L** state:

$$K_L = \frac{\mathbf{k}_0}{D^2 \cos^2\alpha} \qquad (7)$$

If the starting state is **S**, the force f causes a different angular change and K_S can be obtained for small rotations with the $\varphi \to 0$ approximation, after substitution for the **S**-state angle $\beta = \alpha - \Phi$:

$$K_s = \frac{\mathbf{k}_0}{D^2 \cos^2(\alpha - \Phi)} \qquad (8)$$

Finally, the relative change in apparent stiffness between the two states is expressed as

$$\frac{\Delta K}{K_L} = \frac{K_S - K_L}{K_L} = \frac{\cos^2\alpha}{\cos^2(\alpha - \Phi)} - 1 \qquad (9)$$

In Figure 4A $\Delta K/K_L$ is plotted as a function of conformational angle change φ, and with the resting angle α as the parameter. It is apparent that the larger the resting angle, the larger the obtained stiffness change. It is interesting that with a large (e.g., 85°) starting angle, even a very modest conformational angle change provides a large stiffness change, approaching 100%.

The next step is to compute the length change resulting from the elementary motor's conformational angle change Φ. This has been done above for small angle change, but an equation in the same form applies here: $\Delta X = D[\sin\alpha - \sin(\alpha - \Phi)]$. The relative length change of the molecule between the **L** and the **S** states is then obtained:

$$\frac{\Delta X}{X_L} = \frac{X_S - X_L}{X_L} = \frac{\sin(\alpha - \Phi)}{\sin\alpha} - 1 \qquad (10)$$

In Figure 4B, we plot $\Delta X/X_L$ for the same range of α and Φ as was used in Figure 4A, where stiffness changes were examined. Because of the orthogonality of the sine and cosine functions, while large stiffness changes accrued with large starting angles, displacement behaves differently. For a given conformational angle change, the smaller the starting angle, the larger the length change.

Elementary stiffness and length values corresponding to the **L** and **S** states, as computed from the boomerang model, can be substituted into eq. (3) and (4) to compute cell stiffness and length. We now demonstrate how one might obtain parameter values with minimal assumptions using the internal structure of the boomerang model. From eqs. (3), (6), and (7) one can write two relationships for $p_s = 0$ and $p_s = 1$, in which the quantities k_0/D^2 and κ appear. Let us assume that $\alpha = 85°$ and $\beta = 40°$, i.e., the conformational angle change $\Phi = 45°$. Taking representative values of $K_{cell} = 7$ mN m^{-1} at $p_s = 0$ and $K_{cell} = 0.7$ mN m^{-1} at $p_s = 1$, one computes $\kappa = 70.3$ mN m^{-1} and $k_0/D^2 = 0.112$ mN m^{-1} rad^{-1}. With the help of the latter value, the elementary stiffness values in the **L** and **S** states may be computed from eq. (6) and (7) to obtain the values $K_L = 14.8$ and $K_S = 0.19$ mN m^{-1}. A value for the global cell stiffness λ is arbitrarily taken as one-tenth of the cell's resting stiffness, or 0.6 mNm^{-1}. This choice conforms to the ratio of normal axial stiffness and the stiffness of permeabilized cells (Tolomeo et al. 1996). Assuming that $D = 1.0$ nm, the "throw" of the elementary motor is $D(\sin\alpha - \sin\beta) = 0.35$ nm. The rotational stiffness k_0 can also be obtained from the known value of k_0/D^2, and a value of 1.1×10^{-22}N m rad^{-1} results. In the resting state, i.e., at $V = 0$, the second term is computed from eq. (4) as 3.7 μm; thus, the uncontrolled length is chosen as $L_0 = 56.3$ μm to

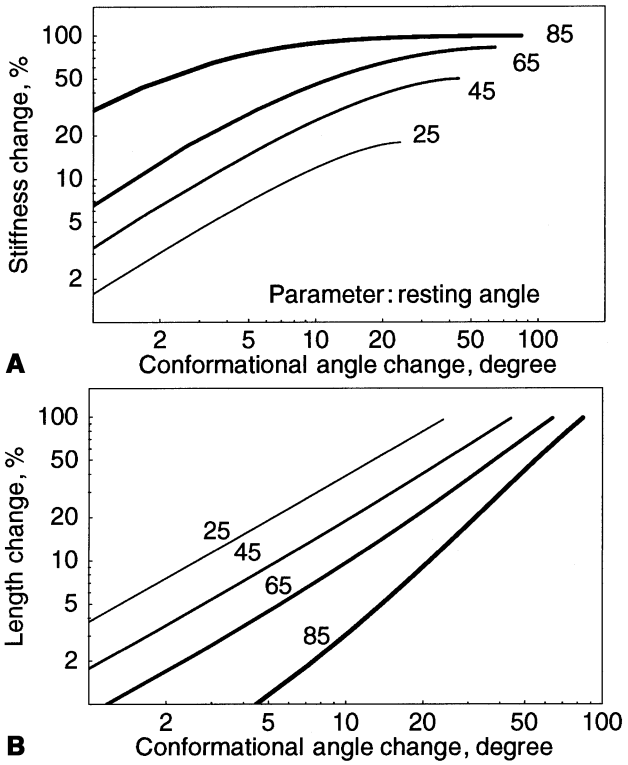

FIG. 4. Boomerang model: **A**. Percentage stiffness change of an elementary motor unit as a function of conformational angle (Φ). The resting angle (α) of the movable arm is the parameter. **B**. Percentage length change as a function of the same variables as above.

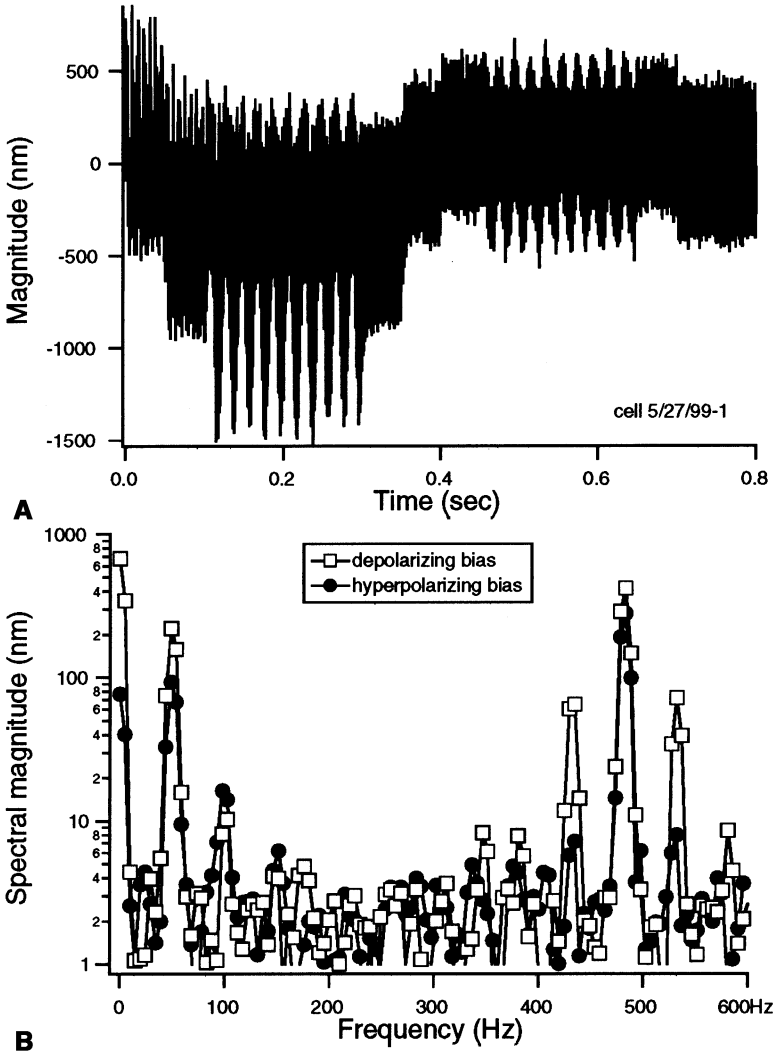

FIG. 5. Experimental results depicting motion of a cell loaded by a driven fiber. **A**. Loaded (by the cell) fiber motion (483 Hz) while electromotile response is elicited by a combination of DC pedestal (first depolarizing then hyperpolarizing, ±100 mV) and 49-Hz sinusoidal command voltage (150 mV p–p). **B**. Fourier spectra of the two halves of the waveforms in **A**. Note the harmonic structure of electromotile response (49, 98, 147 Hz) and intermodulation between fiber motion and electromotility (434 and 532 Hz).Cell length = 70 μm, 75% excluded from microchamber.

yield $L = 60$ μm. As we review computations performed in the first Results subsection, we note that the numbers taken there for K_L and K_S and other parameters were simply the rounded values of those just determined from the boomerang model. Clearly, the graphs presented for cell length and cell stiffness (Fig. 2) well describe the case based on the realization of the elementary motor as the boomerang.

Test of the model

Our experimental results suggest that stiffness changes are sensitive to membrane potential but not to mechanical loading (compression) of the cell. Also, changes in the degree of nonlinearity with hyperpolarization versus depolarization are anything but intuitive. In Figure 5 we present an example where the motile response of an isolated OHC loaded with a flexible glass fiber was examined. In this case, the electrical signal used to elicit motility was a 49-Hz sinusoidal burst superimposed first on a +100-m V and then on a −100-m V−DC pedestal. The loading fiber was sinusoidally driven by a piezo bimorph at 483 Hz. As we have shown before(He and Dallos 1999, 2000), in this mode of two-frequency stimulation, OHC axial stiffness change is modulated at 49 Hz, yielding intermodulation distortion in the joint cell–fiber motion at 434 and 532 Hz. The size of these intermodulation components reflects the magnitude of modulation of the fiber-driven cell compression and expansion and, thus, the modulation of stiffness. The waveform in Figure 5A and its Fourier spectrum in Figure 5B clearly indicate that loaded motile response (at 49 Hz) is greater when elicited on the depolarizing pedestal than on the hyperpolarizing one. It is noted from Figure 5B that the relative harmonic distortion of the electromotile response is greater in the hyperpolarization condition. These behaviors are expected from the shape of the Boltzmann function that represents the motility vs. membrane potential relation(Santos–Sacchi 1989; Evans et al. 1991; Dallos et al. 1993). However, from the Boltzmann function, one expects

a larger response to be accompanied by reduced nonlinearity. Figure 5B clearly shows that this is not the case for intermodulation. Intermodulation distortion (the 434- and 532-Hz components) is considerably greater upon depolarization compared with hyperpolarization. The amplitude of the 483-Hz fiber motion is also greater (smaller) during depolarization (hyperpolarization). This signifies that the DC bias reduced (increased) the cell's (functioning as the load upon the fiber)stiffness. Thus, both the DC and 49-Hz electrical signals modulate the cell's stiffness.

Another test is to use the same paradigm as above but substitute mechanical biasing for the electrical one. In other words, how does intermodulation change when the cell is more or less compressed by the driving fiber? Our data indicate (not shown) that cell compression results in a small change in electromotile amplitude and intermodulation.

The above sets of experimental results can be simulated in the model. If the stiffness of the driving fiber is ρ and its free amplitude is x_1 while the free OHC electromotile response is [as above in eq. (4)] X_{cell} and the cell's stiffness is K_{cell} [eq. (3)], the following describes the loaded response of the cell:

$$X_L = x_1 \frac{\rho}{\rho + K_{\text{cell}}} + X_{\text{cell}} \frac{K_{\text{cell}}}{\rho + K_{\text{cell}}} \qquad (11)$$

Using a simulation of the model via eqs. (3), (4), (7), (8), and (11) one can compute the Fourier spectra of the loaded cell response with both electrical and mechanical biasing. Some results are shown in Figure 6, where Fourier spectra produced by two levels of electrical biasing for the loaded condition [eq. (11)] are presented. The results are striking. Electrical bias strongly influences intermodulation. Hyperpolarization of the cell significantly reduces the two intermodulation components, whereas depolarization increases them. The magnitudes of the fundamental frequency of the electromotile response and the fiber motion change are as expected. These components are reduced by hyperpolarization and increased by depolarization. The relative harmonic distortion of the electromotile response increases with hyperpolarization (the response is more distorted) and decreases with depolarization (the response is less distorted). Thus, the model predicts that distortion (relative harmonic content) in the electromotile response moves in the opposite direction from intermodulation. Depolarization of the cell reduces distortion in the electromotile response but increases the intermodulation with the frequency of the loading fiber. The amount of intermodulation is related to the magnitude of the electromotile response. These findings are in accord with the experimental results (Fig. 5). One can also model the effects of DC mechanical biasing on the loaded response. In accordance with experimental results,

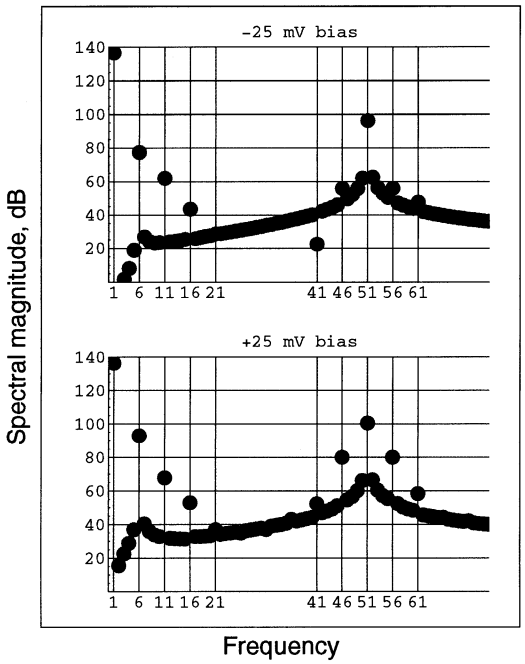

FIG. 6. Simulation of the experimental conditions of Fig. 5, using the same parameters as in previous computations. Spectrum of electromotile response in the loaded condition with two levels of electrical bias. DC, fiber motion, the fundamental frequency of electromotile response and its second and third harmonic, as well as intermodulation frequencies, are marked by vertical lines. The two frequencies used in the simulation are 50 Hz for the fundamental of fiber motion and 5 Hz for the fundamental of electromotility.In the Mathematica Fourier Transform program, DC appears at position 1, 5 Hz at position 6, 50 Hz at 51, etc.

Fourier spectra (not shown) reveal that modest mechanical bias has virtually no effecton either loaded motile response or intermodulation.

DISCUSSION

That OHCs change their length when their membrane potential is altered has been known for more than 15 years (Brownell 1983; Brownell et al. 1985; Kachar et al. 1986). A variety of models have been proposed to explain this motile mechanism (Dallos et al. 1992, 1993, 1997; Iwasa 1993, 1997; Iwasa and Chadwick 1992; Iwasa and Adachi 1997; Kalinec et al. 1992; Santos–Sacchi 1991; Spector et al. 1998; Steele et al. 1993; Tolomeo and Steele, 1998). Most models posit that elementary motor molecules in the cell membrane alter the surface area of the cell, resulting in a predominantly axial length change. Voltage-dependent stiffness change does not naturally follow from any of the ingenious models that have been proposed during the 15 years of research on electromotility. We are suggesting two versions of a model that can provide both length and stiffness changes via the same mechanisms.

Similar to previous work, the first model assumes that a molecule changes its shape upon alteration of the cell's membrane potential. Our modification is that a stiffness change is also assigned to the molecule. The result of an aggregate of large numbers of molecules shifting their state from **L** to **S** is that cell shortens and its axial stiffness decrease. Converse shift produces elongation and stiffening. Graded length and stiffness changes result from the stochastic nature of the molecule's conformation shift and the availability of a large number of molecules, as we proposed before (Dallos et al. 1992, 1993). We emphasize that this is a completely general model, assuming only a combined dimesional and stiffness change of the motor molecule as a stochastic function of membrane potential.

In the second model, an alternative scheme is envisioned. Here we make no assignment of a length change to the molecular motor. Instead, the motor's sole function is to alter its own stiffness, or, in an alternative realization, to switch an elementary stiffness unit in or out. Of course, both stiffness change and switch can be had during the translocation of a charge associated with the motor and, thus, a gating current or nonlinear capacitance is expected (Ashmore 1989; Santos–Sacchi 1991). In this scheme, the only prerequisite for proper functioning of the cell—in other words, for the expression of both stiffness and length changes—is that the cell should be preloaded in its quiescent state. It is as if a spring were compressed by a constant force and then changed its stiffness. As stiffness decreases, the preload is able to further compress the spring, whereas if the stiffness increases, the spring will extend beyond its preloaded, resting-stiffness state. This simple expedient yields cell elongation with increased stiffness and cell shortening with decreased stiffness, as observed. The critical point of this scheme is that the stiffness change is the primary variable. Length change, or electromotility, is a simple consequence of stiffness change. Initial compression may arise from a combination of internal and external constraints. For example, it is conceivable that an interaction between the cortical lattice (Holley and Ashmore 1988) and the cell's infracuticular core structure, that connects the nucleus and the cuticular plate (Kimura 1975), might keep the cell under tension and make it shorter than the neutral length. It also has been shown (Tolomeo et al. 1996) that if the cell membranes are removed by detergent treatment, the cell increases its length. This indicates that the intact cell is prestressed, as required by the model. It is also possible, as shown by Jen and Steele (1987), that a cell with an orthotrophic wall shortens with internal pressure. The circumferential filament structure of the OHC (Holley and Ashmore 1988) combined with its turgor could yield a resting shortened state. Furthermore, *in situ* the cell may be additionally compressed between the reticular lamina and Deiters' cups, thereby intensifying the preload.

Finally, as an example, a specific means of achieving the requirements of the first model was suggested. The chosen approach derives from one envisioned form of conformational change in the motor molecule (Dallos et al. 1992, 1993). Assuming that the motor protein's native configuration is an ℓ-shape and that the activated form has a shallower angle between the arms, length changes can be easily had (Dallos et al. 1993). A requirement is that the molecules are arranged in a relatively uniform orientation *vis-à-vis* the cell's long axis. In other words, this is a decidedly anisotropic configuration. By connecting the two arms elastically, the isomeric shift is accompanied by an *apparent* stiffness change of the molecule, as measured along the cell's long axis [Fig. 3 and eq. (6)].This simple device then confers both length and stiffness change upon the cell. By incorporating stochastic dependence of the molecular configuration upon membrane potential, the nonlinear properties of motility and stiffness change are obtained.

Future models of cochlear micromechanics need to incorporate both OHC voltage-dependent length and stiffness. Some initial work to this effect has been made (Allen 1990).

ACKNOWLEDGMENTS

Supported by the NIDCD, NIH (Grant DC00708). We thank Gulam Emadi for his comments on the manuscript.

REFERENCES

ALLEN JB. Modeling the noise damaged cochlea. In: DALLOS Pt, GEISLER CD, MATTHEWS JW, RUGGERO MA, STEELE CR (eds). The mechanics and biophysics of hearing. Springer-Verlag Berlin. pp 324–332, 1990.

ASHMORE JF, MEECH RW. Ionic basis of membrane potential in outer hair cells of guinea pig cochlea. Nature. 322:368–371, 1986.

ASHMORE JF. A fast motile response in guinea pig outer hair cells: the cellular basis of the cochlear amplifier. J. Physiol. Lond. 388:323–347, 1987.

ASHMORE JF. Transducer motor coupling in cochlear outer hair cells. In: WILSON JP, KEMP DT (eds). Cochlear mechanisms. Plenum Press, London. pp 107–113, 1983.

BROWNELL WE. Observations on a motile response in isolated outer hair cells. In: WEBSTER WR, AITKIN LM (eds). Mechanisms of Hearing. Monash University Press, City. 5–10, 1983.

BROWNELL WE, BADER CR, BERTRAND D, DE RIBAUPIERRE Y. Evoked mechanical responses of isolated cochlear hair cells. Science. 227:194–196, 1985.

DALLOS P, EVANS BN. High frequency motility of outer hair cells and the cochlear amplifier. Science. 267:2006–2009, 1995.

DALLOS P, HE DZZ. Models of outer hair cell stiffness and motility.

In: WADA H, TAKASAKA T (eds). Recent Developments in Auditory Mechanics. World Scientific, Singapore. pp xxx–xxx, 2000.

DALLOS P, HALLWORTH R, EVANS BN. Nature of the motor element in electrokinetic shape changes of cochlear outer hair cells, Nature. 350:155–157, 1991.

DALLOS P, HALLWORTH R, EVANS BN. Stochastic theory of outer hair cell electromotility. In: CAZALS Y, HARNER K, DEMANY L (eds). Auditory physiology and perception. Pergamon Press, Oxford. pp 35–44, 1993.

DALLOS P, HALLWORTH R, EVANS BN. Theory of electrically driven shape changes of cochlear outer hair cells. J. Neurophys. 70:299–323, 1993.

DALLOS P, HE DZZ, LIN X, SZIKLAI I, MEHTA S, EVANS BN. Acetylcholine, outer hair cell electromotility, and the cochlear amplifier. J. Neurosci. 17:2212–2226, 1997.

EVANS BN, HALLWORTH R, DALLOS P. Asymmetries of motile responses of outer hair cells in simulated in vivo conditions. In: WILSON JP, KEMP DT (eds), Cochlear mechanisms. Plenum Press, London. pp 205–206, 1989.

EVANS BN, HALLWORTH R, DALLOS P. Outer hair cell electromotility: the sensitivity and vulnerability of the DC component. Hear. Res. 52:288–304, 1991.

HAMILL OP, MARTY A, NEHER E, SAKMANN B, SIGWORTH FJ. Improved patch-clamp techniques for high-resolution current recording from cells and cell-free membrane patches. Pflügers Arch. 391:85–100, 1981.

HE DZZ, DALLOS P. Somatic stiffness of cochlear outer hair cells is voltage-dependent. Proc. Natl. Acad. Sci. USA. 96:8223–8228, 1999.

HE DZZ, DALLOS P. Properties of voltage-dependent axial stiffness of cochlear outer hair cells. JARO. 1:164–81 2000 10.1007/s101620010006

HOLLEY MC, ASHMORE JF. On the mechanism of high frequency force generator in outer hair cells isolated from guinea pig cochlea. Proc. R. Soc. B Biol. Sci. 232:413–429, 1988.

IWASA KH. Effect of stress on the membrane capacitance of the auditory outer hair cell. Biophys. J. 65:492–498, 1993.

IWASA KH. Current noise spectrum and capacitance due to the membrane motor of outer hair cell: A theory. Biophys. J. 73:2965–2971, 1997.

IWASA KH, CHADWICK RS. Elasticity and active force generation of cochlear outer hair cells. J. Acoust. Soc. Am. 92:3169–3173, 1992.

IWASA KH. Effect of membrane motor on the axial stiffness of the cochlear outer hair cell. J. Acoust. Soc. Am. 107:2764–2766 2000 10.1121/1.428663

IWASA KH, ADACHI M. Force generation in the outer hair cells of the cochlea. Biophys. J. 73:546–555, 1997.

JEN DH, STEELE CR. Electrokinetic model of cochlear hair cell motility. J. Acoust. Soc. Am. 82:1667–1678, 1987.

KACHAR B, BROWNELL WE, ALTSCHULER RA, FEX J. Electrokinetic shape changes of cochlear outer hair cells. Nature. 322:365–368, 1986.

KALINEC F, HOLLEY M, IWASA K, LIM D, KACHAR BA. Membrane-based force generation mechanism in auditory sensory cells. Proc. Natl. Acad. Sci. USA. 89:8671–8675, 1992.

KIMURA RS. The ultrastructure of the organ of Corti. Int. Rev. Cytol. 42:173–222, 1975.

SANTOS–SACCHI J. Asymmetry in voltage-dependent movements of isolated outer hair cells from the organ of Corti. J. Neurosci. 9:2954–2962, 1989.

SANTOS–SACCHI J. Reversible inhibition of voltage-dependent outer hair cell motility and capacitance. J. Neurosci. 11:3096–3110, 1991.

SPECTOR AA, BROWNELL WE, POPEL AS. Elastic properties of the composite outer hair cell wall. Ann. Biomed. Eng. 26:157–165, 1998.

STEELE CR, BAKER G, TOLOMEO J, ZETES D. Electromechanical models of the outer hair cell. In: H. DUIFHUIS, JW. HORST, P. VAN DIJK, SM. VAN NETTEN (eds). Biophysics of hair cell sensory systems. World Scientific, Singapore pp 207–215, 1993

TOLOMEO JA, STEELE CR. A dynamic model of cell motility including intracellular and extracellular viscosity. J. Acoust. Soc. Am. 103:524–534, 1998

TOLOMEO JA, STEELE CR, HOLLEY MC. Mechanical properties of the lateral cortex of mammalian auditory outer hair cells. Biophys. J. 71:421–429, 1996